Directed Aqueous-Phase Reforming of Glycerol Through Tailored Platinum Nanoparticles

J. Callison[a,b*], N. D. Subramanian[a,b], S. M. Rogers[a,b], A. Chutia[a,c], D. Gianolio[d], C. R. A. Catlow[a,b,e], P. P. Wells[a,d,f*] and N. Dimitratos[e*]

[a]UK Catalysis Hub, Research Complex at Harwell, Rutherford Appleton Laboratory, Harwell, Oxon OX11 0FA, United Kingdom.
[b]Department of Chemistry, University College London, 20 Gordon Street, London WC1H 0AJ, United Kingdom.
[c]School of Chemistry, University of Lincoln, Brayford Pool, Lincoln, Lincolnshire LN6 7TS, United Kingdom.
[d]Diamond Light Source Ltd, Harwell Science and Innovation Campus, Chilton, Didcot OX11 0DE, United Kingdom.
[e]Cardiff Catalysis Institute, School of Chemistry, Cardiff University, Cardiff CF10 3AT, United Kingdom.
[f]University of Southampton, University Road, Southampton SO17 1BJ, United Kingdom.
[*]Corresponding authors: june.callison@rc-harwell.ac.uk, ppwells@soton.ac.uk, DimitratosN@cardiff.ac.uk

Abstract

Sustainable technologies require both renewable feedstocks and catalysts that are able to direct their conversion to specific products. We establish a structure-activity relationship for the aqueous phase reforming of glycerol over 2% Pt/Al_2O_3 catalysts, whereby the reaction pathway can be controlled to produce either hydrogen or 1,2-propanediol as the main product. Using the colloidal synthesis method, the reduction temperature was altered to produce Pt nanoparticle catalysts supported on Al_2O_3 with varying Pt particle size. The catalytic activity of the samples for the APR of glycerol resulted in a higher conversion of glycerol (34%) for the larger Pt particle size of ~3.5 nm, producing the liquid 1,2-propanediol as the major product with a yield of 12.5%, whereas smaller particles of ~2.2 nm gave hydrogen as the main product (5.5% yield). This work demonstrates how the APR of glycerol can be tuned to yield both valuable liquid and gas products using tailored Pt nanoparticles.

1. Introduction

1.1. Glycerol as a By-Product

The production of crude glycerol has increased significantly in recent years as a consequence of the rapid growth in the production of biodiesel as an alternative for petroleum-based fuels. Finding a commercially viable use for this ‘waste’ glycerol, the main by-product in the production of biodiesel, is now an active area of research, with many possible applications [1–7]. The production of hydrogen, coupled with liquid-phase products, through aqueous phase reforming (APR) of glycerol, is one possible route. A clean and

sustainable supply of hydrogen is required to enable a future hydrogen economy, an example being the development of proton exchange membrane fuel cell technology [1,2]. The current industrial processes used to produce hydrogen involve the reforming of hydrocarbons, resulting in high CO_x emissions and adding to the depletion of fossil fuel reserves [2,8].

1.2. Aqueous Phase Reforming

Aqueous phase reforming of glycerol, shown in equation (1), was highlighted in 2002 by Dumesic [8] as a promising method for the production of hydrogen as it is both kinetically and thermodynamically favourable. It can be carried out at relatively low temperatures, ~227°C, it minimises undesirable side reactions, and facilitates the water gas shift reaction (WGS) (equation (2)), limiting the production of CO, known to poison $H_{2(g)}$ fuel streams [1,3,4,9,10].

$$C_3H_8O_3 + 3H_2O \leftrightarrow 7H_2 + 3CO_2 \quad (1)$$

$$CO + H_2O \leftrightarrow CO_2 + H_2 \quad (2)$$

1.3. Glycerol to Hydrogen

Recent studies have shown that Pt based catalysts have high activity and selectivity compared to other monometallic systems for the APR of glycerol [4,8,11–13]. Despite its expense, Pt is a favourable choice as a consequence of its enhanced ability to cleave C-C bonds and promote the WGS reaction [9,14]. The support material has also shown to affect the catalytic activity; Guo *et al.* studied a range of supports and found that Pt supported on γ-Al_2O_3 gave a higher rate of production of H_2 compared to SiO_2, TiO_2 and CeO_2, which was ascribed to the higher basicity of the Al_2O_3 support [1].

Thus far the majority of studies on glycerol APR has been on commercial catalysts or those produced via classic synthesis methods such as impregnation and precipitation. However, recent work has shown that an increase in activity can be achieved by using supported nanoparticles prepared using colloidal synthesis methods [15–17]. Bönnemann *et al* concluded that improvement of catalytic activity from a colloidal system was due to the fact that metal nanoparticles prepared by the this method occupy the most exposed sites of a support, rather than being buried under the surface [15].

Compared to the classic synthesis methods, sol-immobilisation techniques afford the possibility of fine-tuning the properties of supported metal nanoparticles, thereby allowing greater control of the size, shape and dispersion in the final catalyst [18–20]. This is achieved

by the use of a stabilizing agent during the synthesis, such as polyvinyl alcohol, (PVA), leading to more well dispersed catalysts with narrow particle size distribution [15,21,22].

Recent studies used variation of the colloidal reduction temperature and solvent systems during synthesis to modify gold and palladium nanoparticles for use in the oxidation of glycerol and hydrogenation of furfural, respectively. These studies proved that the colloidal synthesis technique can be used to control the size of the metal nanoparticles and the proportion of available active surface sites, resulting in changes in selectivity [20,23].

1.4. 1,2-Propanediol Production

The main focus in the published literature on the APR of glycerol has been the production of hydrogen. However, a high yield of liquid products are also formed from a complex network of reactions. These products also have significant applications, for instance 1,2-propanediol (1,2-PDO), produced from the hydrogenolysis of glycerol under APR conditions, is used in the food, cosmetic and pharmaceutical industries [24,25].

Currently 1,2-Propanediol is commercially produced via the hydration of propylene oxide derived from propylene. Renewable feedstock can be used to produce 1,2-PDO by hydrogenolysis however this pathway requires high temperatures and pressures. For instance, studies on the conversion of glycerol have required pressures upwards of 100 bar and an external hydrogen source, therefore making this an expensive process to consider commercially viable [26].

It has been shown that using APR conditions, glycerol can be converted to 1,2-PDO via an acetol pathway, generating hydrogen in situ and has been proposed as a potential alternative to the one step hydrogenolysis [27].

Due to its active nature for the APR of glycerol, Pt nanoparticles supported on γ-Al_2O_3 was chosen for this study as a model catalyst. The colloidal synthesis method was used to generate preformed Pt nanoparticles with specific morphology to obtain structure-activity relationships in an attempt to improve the catalytic activity and control the reaction pathway to favour either hydrogen or 1,2-propanediol, using optimised conditions that we have recently reported [13].

2. Experimental

2.1. Catalyst preparation

Pt/Al_2O_3 catalysts were prepared using the sol-immobilization method based on a previous experimental regime to produce Pt and Au colloidal systems [20,28]. A stock solution containing the precursor, K_2PtCl_4 (99.99%, Aldrich), was added to distilled water (Pt concentration = 1.03 – 2.05 x 10^{-4} M) that had been heated to the desired temperature (25 – 90°C) using a stirrer/hotplate. For the synthesis at 90°C a reflux condenser was used to keep the solution in the liquid phase. Poly(vinyl alcohol) (PVA, Aldrich, Mw = 9000 – 10000 g mol^{-1}, 80% hydrolysed, PVA/Pt (wt/wt) = 0.65) was added in order to stabilise the solution. A freshly prepared solution of the reducing agent, $NaBH_4$ (0.1 M) (>96%, Aldrich, $NaBH_4$/Pt (mol/mol) = 5 - 10) was added drop wise with stirring to form a black sol. The Al_2O_3 support material (Aeroxide AluC, Degussa) was then added and the solution stirred vigorously. After a period of time the solution was filtered, washed extensively with distilled water to remove any precursor material and dried overnight at room temperature [29].

The colloidal solutions were monitored throughout the synthesis procedure by UV-vis spectroscopy (Shimadzu UV-1800 spectrometer with Quartz cells) to assess the reduction of the Pt precursor.

2.2. Catalyst characterisation

The Pt loading of the samples was determined by both Microwave Plasma - Atomic Emission Spectrometry (MP-AES) and Energy Dispersive X-ray Spectroscopy (EDS). For MP-AES analysis, the solid samples (0.1g) were digested in aqua regia using an Anton Paar Multiwave 3000 and diluted in deionised water to form a 0.1 wt% solution. The elemental analysis was performed using an Agilent 4100 MP-AES. Pt standards were made up in 10% aqua regia and used to calibrate the instrument before the samples were run. EDS analysis was performed on a JSM-6610LV scanning electron microscope (JEOL) fitted with Oxford Instruments Xmax 80mm EDS detector running Aztec analysis software. The powder samples were dispersed on conductive carbon tabs placed on aluminium stubs.

Transmission Electron Microscopy (TEM) was used to investigate the particle size and dispersion of the metal nanoparticles on the Al_2O_3 support. Analysis was carried out on a JEM-2100 Plus electron microscope with a 200 kV accelerating voltage. Samples for TEM were prepared by dispersing the supported catalysts in methanol and then dropping the solution on 300 mesh carbon-coated copper grids.

The surface area of the samples was measured using the Brunauer Emmett Teller (BET) method. The samples were first degassed at 140°C under vacuum using a FloVac Degasser. Analysis was then carried out on a Quadrasorb EVO instrument supplied by Quantachrome.

X-ray diffraction (XRD) patterns were recorded on a Rigaku Miniflex 600 benchtop powder X-ray diffractometer equipped with a 6-position autosampler and Cu Kα radiation source. The 2θ angles were scanned from 5 to 80˚ at a rate of 5˚/min. The average Pt crystallite sizes were calculated using the Scherrer equation for the Pt (111) diffraction peak at 2θ = 39.9˚ [30].

X-ray Absorption Fine Structure (XAFS) studies were carried out on the Pt L_3-edge on the B18 beamline at the Diamond Light Source, Didcot, U.K. Measurements were performed in transmission mode using a QEXAFS setup with a fast-scanning Si(111) double crystal monochromator and ion chamber detectors. An average of 6 scans were acquired and merged to help improve the signal-to-noise level of the data. The time resolution of the spectra was 1 min/spectrum (k_{max} = 18). Fresh catalyst samples were analysed as synthesised and after reduction under hydrogen at room temperature. Used catalyst samples were washed with water and dried at 120°C in static air overnight before analysis.

The software used to carry out the XAS data processing and the extended X-ray absorption fine structure (EXAFS) analysis was IFEFFIT with the Horae package (Athena and Artemis) [31,32]. The typical fit range for the EXAFS data was 1.1 < R < 6Å and 3.1 < k < 15.3.

CO adsorption studies were performed on both fresh and used catalyst samples using transmission Fourier Transform Infrared Spectroscopy (FTIR). The used samples were washed with distilled water and dried in an oven overnight at 120°C to remove as much of the reaction solution as possible. 25 – 30 mg of sample was pressed into a self-supporting pellet and mounted in a Harrick Dewar transmission/reflection accessory. The FTIR spectra were obtained with a Thermo Scientific Nicolet iS10 spectrometer at a spectral resolution of 4 cm^{-1} and accumulating up to 64 scans. For each experiment, the sample cell was purged with helium at 80 cm^3 min^{-1} and heated to 270°C where the sample was reduced by flowing a mixture of 50% H_2/He for 30 minutes. The sample was then cooled to ~30°C in helium, whereby a spectrum was recorded to use as a background scan. CO was then introduced using a 10% CO/He mixture at a flow rate of 80 $mlmin^{-1}$ for 30 seconds, which was repeated until the spectrum showed that the surface of the sample was saturated with CO. The sample was

then flushed with helium to remove gaseous and physisorbed CO from the catalyst surface and the final spectra recorded after 30 minutes. The background spectrum was then subtracted to give the final spectrum.

ATR-FTIR spectra were collected on the catalyst samples using a Smart iTR Attenuated Total Reflectance sampling accessory. Spectra were collected at a spectral resolution of 2 cm^{-1} and accumulating up to 64 scans.

2.3. Catalytic tests

The APR of glycerol was carried out in a 50 ml autoclave batch reactor (Parr Series 4590 Bench Top Micro Reactor equipped with magnetic drive stirrer and a Parr 4848B Reactor Controller system) using experimental conditions optimized and reported in a previous study [13]. Typically, 60 mg of catalyst was added to 20 ml of 10 wt% aqueous glycerol solution (corresponding to substrate to metal ratio of 4935 and a glycerol to water molar ratio of 0.022) and the solution purged with argon in the sealed reactor. The reactions were carried out at 1000 rpm, 240°C ± 2°C and 42 ± 1 bar (argon). Gas products were collected in a gas sampling bag after the reaction had been cooled and analysed using a Shimadzu gas chromatograph system (GC-2014 with TCD and FID), equipped with Hayesep N and Mol Sieve 5A packed columns (2M x 1/8”). The concentration of unreacted glycerol and the main liquid products were analysed using a Shimadzu Prominence HPLC installed with a MetaCarb 67H column, SPD-M20A Photodiode Array UV-Vis detector and a RID-10A refractive index detector. The quantification of the reactants and products were carried out using external calibration methods for both the gas and liquid analysis to allow calculation of the moles produced. The product concentrations calculated had an error of ± 4% due to analytical error. The glycerol conversion was calculated according to the following definition

$$\text{Glycerol Conversion (\%)} = \frac{C_0 - C_t}{C_0} \text{ x } 100$$

The selectivity’s of the products are reported in the ESI and were calculated as follows:

$$\text{Hydrogen Selectivity (\%)} = \frac{\text{Molecules of } H_2 \text{ produced}}{\text{C atoms in gas products}} \text{ x } \frac{1}{R} \text{ x } 100$$

Where R is the H_2/CO_2 reforming ratio of 7/3 for glycerol.

$$\text{Product Selectivity (\%)} = \frac{\text{C atoms in product}}{\text{C atoms converted}} \text{ x } 100$$

Reusability of the catalyst samples was also tested using the reaction conditions above. After one two-hour cycle, the glycerol conversion was determined and used to calculate the amount of glycerol required to be added to produce a 10% feed solution. The procedure was then repeated until 5 reaction cycles had been carried out.

The APR reactions of hydroxyacetone, 1,2-propanediol, lactic acid and glyceraldehyde were carried out using the same experimental conditions as with glycerol, using a 1 – 10 wt% reactant solution in water and 1-hour time-on-stream to determine and elucidate reaction pathways.

Potential metal leaching into the reaction mixture was also analysed using MP-AES analysis. For this, concentrated HCl (>=37%) was added to the spent reaction solution after filtering to produce a 10% HCl solution. Calibration standards were also made in 10% HCl. The minimum detection limit of the MP-AES instrument using this method was 10ppb.

3. Results and discussion

3.1. Synthesis of 2% Pt/Al_2O_3 catalysts

In order to ensure accurate comparison for the reactivity and characterisation of the synthesised catalysts, the colloidal synthesis method for the production of Pt nanoparticles was first optimised by a series of systematic studies, which ensured the catalyst samples were of sufficient Pt loading and the synthesis method was reproducible. The variables investigated in this study were: the concentration of the reducing agent ($NaBH_4$), the reduction time of the Pt precursor and the immobilisation time on the support. To achieve complete immobilisation, it was found that the timescales required for the reduction and immobilisation were both 24 hours. In the reduction stage of the synthesis, the production of Pt(0) colloids was demonstrated by following the ligand field induced transitions for the $PtCl_4^{2-}$ anion [33] demonstrated in Figure 1. Pt(0) colloids have a broad steeply rising absorption around 200 nm as a result of longitudinal dipole resonances, which is consistent with previous studies [28,34]. Following the reduction of $PtCl_4^{2-}$ as a function of time, it was clear that 4 hours was insufficient to achieve complete reduction; $PtCl_4^{2-}$ ligand field transitions are readily visible in the UV-Vis spectrum of the colloidal solution, which results in poor immobilisation and the bands are also present in the filtrate after supporting on Al_2O_3. Increasing the reduction time to 24 hours results in a UV-Vis spectrum which is consistent with colloidal Pt and improved immobilisation. MP-AES results confirmed this improvement

as the measured Pt loading of the sample reduced for 24 hours was 1.53 wt%, compared to 1.15 wt% for the sample reduced for 4 hours.

Using this optimized synthesis procedure, catalysts were then produced at four different reduction temperatures, 25°C, 50°C, 75°C and 90°C. Our previous work has shown that by altering the reduction temperature, the resultant size of the metal nanoparticle can be controlled [20,23]; lower reduction temperatures have been found to achieve smaller particles. The prepared samples were labelled Pt25, Pt50, Pt75 and Pt90, respectively. Information of the BET surface area and metal loading are shown in Table S1. The SEM-EDX analysis of the samples showed no evidence of K, Na or B leftover from the precursor materials, with only trace amounts of Cl therefore it is not expected that these elements will affect the studies presented here.

3.2. Characterisation of 2% Pt/Al_2O_3 catalysts

To assess the particle size of the Pt based catalysts three different complimentary techniques: EXAFS, TEM, and XRD, were used (Table 1). The XRD data (Figure 2A, Figure S1), shows a reflection at 2θ=40°, which corresponds to the Pt (111) plane and can be used as a reference peak to show the variation of Pt nanoparticle size [35,36]. As seen in Figure 2A, the Pt diffraction peak is at its lowest intensity for the Pt25 sample and increases with increasing colloidal reduction temperature, indicative of an increase in crystallite size. Using the Scherrer equation [37], this size was calculated for all four samples (Table 1) and found to be 2.25 nm (Pt25), 2.88 nm (Pt50), 3.48 nm (Pt75) and 3.61nm (Pt75), confirming the trend discussed.

The EXAFS data, presented in Table 1 and Figure 2B, shows the same trend as the XRD with regards to increasing particle size. The features between 2 – 3 Å are indicative of 1^{st} shell Pt-Pt scattering paths and it is clear that the magnitude of these peaks increase with increasing synthesis temperature. This corresponds to a greater 1^{st} shell Pt coordination number and by inference a larger particle size. Before analysis, all four samples were reduced in hydrogen at room temperature in order to ensure a fully metallic state, thereby allowing accurate comparison 1^{st} shell coordination numbers.

Using the coordination number obtained from the EXAFS fitting (Figure S2, Table S2), particle sizes could be calculated using published models [38]. The method used assumes that the nanoparticles are spherical, fcc and <3 nm and is limited to 1^{st} shell coordination numbers below 10, therefore the size of the Pt75 and Pt90 catalysts could not be determined through

EXAFS. The results calculated were 1.54 and 1.97 nm for the Pt25 and Pt50 samples respectively.

The TEM analysis, shown in Figure 3, of the Pt25 sample shows the presence of small Pt nanoparticles with good dispersion; however the Pt50 sample starts to show an increased degree of agglomeration, which is also evident in the Pt75 and Pt90 samples where agglomeration is more pronounced. The agglomeration limited the ability to determine an accurate particle size through TEM for the Pt50, Pt75 and Pt90 samples, however, the Pt25 sample was calculated at an average of 2.14 nm.

On comparison of all three techniques, XRD gives the largest particle size for the values given, which as diffraction from the smaller particles is not observed with consequent heavy weighting to larger crystallites. The EXAFS data, however, probes the full range of particles in the sample and is therefore more appropriate for demonstrating trends. The TEM data falls in between as it is limited by the resolution of the microscope (in this instance <1 nm). However, all techniques have their limitations and the ability to use all three in conjunction provides confidence for the trend established here; that as the colloidal reduction temperature is increased, larger Pt particle sizes are formed.

3.3. Activity testing

The series of Pt/Al_2O_3 catalysts prepared were used to establish a structure-activity correlation in the aqueous phase catalytic reforming (APR) of glycerol. Catalytic screening was carried out under batch conditions using an established testing procedure, where a range of products were identified [13]. The products seen in the gas phase were hydrogen, carbon dioxide and methane. Liquid products identified in the reactions were hydroxyacetone (HA), 1,2-propanediol (1,2-PDO), lactic acid (LA), ethanol (EtOH), 1-propanol (1-PrOH), ethylene glycol (EG), acetic acid (AA), glyceraldehyde (GA), 2-Propanol (IPA) and 1,3-propanediol (1,3-PDO), which is in line with previous studies [9,39,40].

Figure 4 shows the glycerol conversion after 2 hours reaction time. The Pt25 catalyst showed the lowest conversion of all the samples, with a conversion of ~12%. This is in line with previous studies on a commercial $2\%Pt/Al_2O_3$ catalyst that showed a conversion of 13% [13]. The Pt50 catalyst performs only slightly better with the most active catalyst being Pt75 (34% conversion). This trend suggests an increase in conversion with mean particle size of Pt, however, a further increase in particle size (Pt90 sample) results in reduced performance. This result can be rationalised by comparing the competing influences of specific activity and

mass activity; normalised to Pt surface area the larger particles would be significantly more active, however, as the Pt mass is kept constant the performance ultimately tails off because of a reduced number of active sites.

For these reactions the hydrogen yield was also calculated (Figure 4), and as the particle size increases, with the Pt75 and Pt90 samples, the hydrogen yield decreases. Therefore, assessing the glycerol conversion and hydrogen yield after 2 hours reaction time allows us to establish that larger Pt particles tend towards higher conversion yet yield reduced levels of H_2. In light of these results, it was clear that more work was required to explore the other products involved in the reaction and to establish reaction pathways.

3.4. Product analysis

To understand more about these structure-property correlations, the Pt25 and Pt75 catalysts were chosen for further detailed investigation; Pt25 achieved the maximum hydrogen yield and the Pt75 showed the maximum glycerol conversion. Full analysis of the liquid products was carried out and the reaction was repeated at several timed intervals at an attempt to understand better the reaction profiles of both catalysts.

Figure 5 shows the glycerol conversion and the amount of gas products formed from both the Pt25 and Pt75 catalysts as a function of time (15 – 480 minutes of reaction time). The conversion for the Pt25 catalyst reaches a maximum of ~12% after 2 hours; however, both H_2 and CO_2 continue being produced, indicating further reactions are taking place. The absence of CO and minimal methane production is in line with thermodynamic studies carried out by Luo [41] whereby the temperature used reduces the external energy input, favouring the water gas shift reaction, but is high enough to favour aqueous reforming over methanation.

The main liquid products (Figure 6) of the Pt25 catalyst after 2 hours are HA and 1,2-PDO; after this time the amount of hydroxyacetone decreases to close to zero, whereby the amount of LA formed increases. Ethanol is also seen as a product up to 2 hours, but levels were found to decrease when tested at 6 hours. These results are indicative that a complex network of reactions are taking place during the APR of glycerol. Two separate reactions pathways are presented in Scheme 1 (route 1) and Scheme 2 (route 2), which are in agreement with previous studies [9] and the results presented here.

For the Pt25 catalyst we propose that route 1 is favoured up to 2 hours, as this is consistent with the products identified: H_2, CO_2, EG and EtOH. After this time, glycerol

conversion ceases and, here the conversion of the HA that has been produced (route 2) becomes dominant, with the main products being H_2, 1,2-PDO and LA.

The Pt75 catalyst, however, showed a different trend, whereby after 2 hours of reaction the conversion of glycerol continued to increase progressively from 34% to 48% conversion. There was a substantial change in the products formed during the time online studies, with a significantly different product distribution compared to Pt25; the Pt75 catalyst showed a lesser amount of gas products, in particular H_2, whereas more liquid products were produced. The H_2/CO_2 ratio for the Pt75 catalyst after 2 hours was 0.5, much lower than the Pt25 catalyst (1.2) and further away from the ideal ratio of 2.3. The major products of Pt75 were HA, LA, and 1,2-PDO; consistent with the pathway route 2 (Scheme 2). Based on the evidence presented here, it is postulated that H_2 is more readily formed in the presence of smaller Pt particles.

The Pt75 catalyst resulted in a more complex distribution of products after 8 hours, with many unidentified trace products evidenced in the HPLC analysis. This is shown in the carbon mass balance data (Table S4), whereby the carbon mass balance of the 8 hour reaction with the Pt25 catalyst was 67%, whereas all the other reactions carried out with the Pt75 and Pt25 catalysts showed a mass balance of >90%. The liquid analysis clearly shows that there are many competing reactions, and that whilst the Pt25 catalyst favours the production of hydrogen, the presence of larger Pt nanoparticles in the Pt75 catalyst favour the production of the oxygenated liquid products. This is a significant discovery, as previous work on this reaction has focused on the production of H_2, ignoring the value in the liquid products such as 1,2-PDO.

3.5. Insights into reaction pathways

To understand further and elucidate the competing reactions and the formation of oxygenated liquid products, we studied the conversion of the following substrates: hydroxyacetone (HA), 1,2-propanediol (1,2-PDO), lactic acid (LA) and glyceraldehyde (GA). The reactions were carried out using the same experimental conditions as the APR of glycerol, using the Pt25 catalyst.

Table 2 shows the reactant conversions for the intermediate reactions in comparison to the reaction with glycerol. The major gas and liquid products formed in the intermediate reactions are shown in Figure 7.

The conversion of hydroxyacetone (53%) was higher than that of glycerol (9%), followed by 1,2-propanediol (22%); indicating that both HA and 1,2-PDO will readily react as intermediates in the APR of glycerol, which is in agreement with our time online studies where both HA and 1,2-PDO formation drops after 2 hours reaction time when glycerol stops converting. 1,2-PDO is the most abundant product in the liquid phase when HA was used as the substrate. This outcome was achieved without any external supply of hydrogen; as 1,2-PDO is produced from the addition of hydrogen to HA (Equation 3), the hydrogen required must have been produced *in situ* from the reformation of HA in agreement with previous reports, whereby HA is broken down to form H_2, CO_2 and methane [9].

$$C_3H_6O_2 + H_2 \leftrightarrow C_3H_8O_2 \qquad (3)$$

1,2-PDO was not produced by any other reactant, suggesting that 1,2-PDO was mainly formed from glycerol via HA as the main intermediate. Moreover, the amount of 1,2-PDO was significantly lower (0.6 mmol) when glycerol was used as the reactant at the same reaction time. These results indicate that the reaction rate of HA conversion to 1,2-PDO is faster than glycerol conversion to 1,2-PDO. Thus, the dehydration of glycerol to HA is one of the limiting factors in the formation of 1,2-PDO from glycerol. Once HA is formed, it quickly undergoes subsequent reactions.

When 1,2-PDO was used as the substrate, a significant amount of HA was observed, confirming that the hydrogenation of HA is reversible. However, the lower conversion of 1,2-PDO compared with that of HA indicates that the reverse reaction is much slower.

The production of alcohols, namely, ethanol (EtOH) and 1-propanol (1-PrOH), is seen in the APR of HA and 1,2-PDO. Ethanol is produced from 1,2-PDO as given by Equation 6, or directly from HA hydrogenolysis/decarbonylation (Equation 7) [27]. These reactions lead to the formation of methane as a by-product, which we see in both the reforming reactions of HA and 1,2-PDO, verifying these reaction pathways.

$$C_3H_8O_2 + 2H_2 \leftrightarrow C_2H_5OH + CH_4 + H_2O \qquad (6)$$

$$C_3H_6O_2 + 3H_2 \leftrightarrow C_2H_5OH + CH_4 + H_2O \qquad (7)$$

We observed the formation of acetic acid, mainly from the reforming of hydroxyacetone and glycerol. According to previous studies acetic acid is formed via C-C cleavage to acetaldehyde followed by dehydrogenation [42,43].

Lactic acid (LA) is shown to be produced from both HA and glyceraldehyde (GA). The formation of LA from GA is crucial as this indicates that from the routes suggested by Wawretz *et al* (Scheme 1), route 1B is favoured using the Pt25 catalyst. A small amount of ethanol is also seen from the glyceraldehyde and the lactic acid reactions, confirming further that ethanol can be produced from glycerol via glyceraldehyde and lactic acid, producing H_2 and CO_2 in the process. The glyceraldehyde reforming reaction in our studies showed 100% conversion after 1 hour, hence the reason why only trace amounts of GA are seen in the glycerol reforming reactions.

From the timed studies in Figure 6, it appears that only a small amount of lactic acid is formed from the glyceraldehyde route for the Pt25 catalyst. However, after glycerol stops converting at 2 hours, the lactic acid amount increases significantly as it is now formed from hydroxyacetone, which suggests that the catalytic species/sites in Pt25 responsible for the conversion of glycerol become inactive after 2 hours, allowing a secondary site to then convert the HA already formed. From the results shown in section 3.4, it was evident that the small particles are responsible for the APR of glycerol to produce H_2 whereas the larger particles favour the liquid products.

3.6. Investigation of catalytic sites

From the studies on the intermediate reactions in the APR of glycerol, it is suggested that different sites on the Pt/Al_2O_3 catalyst are responsible for different reaction pathways. One potential site is the Al_2O_3 support; therefore, reactions were carried out with both glycerol and hydroxyacetone using the bare support material. A blank reaction with hydroxyacetone was also carried out for comparison.

The conversion from the glycerol reaction (table S5 in the ESI) was less than 1%, indicating that Al_2O_3 promotes barely any reaction and that the Pt metal is required to 'activate' the glycerol. The hydroxyacetone however showed a conversion of 40% in the presence of bare alumina and the same in the blank reaction. We can therefore ascribe that post 2 hours in the time online studies of Pt25 the conversion of HA is ascribed not to the presence of catalyst but to the APR reaction conditions. The products that were analysed from the alumina reaction are shown in Figure 8. These results again are similar to the blank reaction (table S5 in the ESI) and show that CO_2 and acetic acid were the main products, with the alcohols ethanol and 1-PrOH also being produced, suggesting that hydrogenolysis and reforming of the hydroxyacetone is taking place under the APR conditions used in this work.

3.7. Catalyst reusability

Due to the relatively harsh conditions used in the APR of glycerol, deactivation of the catalyst is a known issue that has not been widely studied [44]. A commercial 2% Pt/Al_2O_3 catalyst provided by Johnson Matthey was previously tested where it was found that the activity dropped by ~35% after 5 cycles with no treatment to the catalyst in between reactions. The hydrogen yield decreased more dramatically, by ~80% [13].

Figure 9 shows the reusability test results for the Pt25 and Pt75 catalysts. The conversion for the Pt25 sample showed the same trend as the commercial catalyst (Figure S5), whereby the activity increased after the first run then decreased steadily. The drop in activity from the second to the fifth run is ~32%, similar to the previous study [13]; however the decrease in hydrogen yield was not as prominent, decreasing steadily by ~45% overall. During the timed studies we observed that the Pt25 catalyst stops converting after 2 hours however here it is able to 'reactivate' in between each run, which we propose that this is due to the cooling down and reheating of the samples and the exposure to air in between reactions, which can lead to removal of blockages on the active site or even restructuring of the nanoparticles on the surface of the catalyst, a phenomenon that has been modelled by Wei [45]. Deactivation of the catalysts may also be due to the instability of the support material under APR conditions as Al_2O_3 is known to convert to boehmite (discussed in section 3.8). The presence of glycerol has been shown to slow down this conversion however may warrant further investigation in future work [46]. Pt sintering may be another cause of deactivation. In our work no evidence of Pt was found in the reaction solutions down to 10ppb, therefore no indication of metal leaching was found

3.8. Characterisation of catalysts after reaction

CO adsorption studies were performed on both the Pt25 and Pt75 fresh and used catalysts to gain a better understanding of the surface sites, Figure 10 shows the resulting spectra indicating the CO chemisorbed on the catalyst surface. Table 3 summarises the assignments for the peaks identified from each sample.

The peaks at 2062 and 2084 cm^{-1} are attributed to linear CO on edge sites and crystalline Pt (111) sites respectively [47,48]. As expected the smaller particles in the Pt25 fresh catalyst show a higher number of edge sites. However, on the used catalyst, the number of edge sites has decreased, which could indicate either (i) there has been a loss of small sites due to a change in morphology or (ii) the edge sites have been blocked during the reaction. This result

can be linked to the activity testing, whereby after 2 hours it appears the smaller particles responsible for the APR of glycerol are inactive.

For the Pt75 catalyst, both the fresh and used samples show one main peak at ~2090 cm^{-1} for the crystal Pt sites, confirming that the Pt75 sample contains larger Pt nanoparticles with less edge sites. This peak is also shifted to a higher frequency compared to the Pt25 catalyst, which can be indicative of increasing surface coverage as a result of the larger particles [48].

The peak at 1838 cm^{-1} in the Pt25 samples can be attributed to bridging CO that is bound to more than one platinum atom [48]. This peak has clearly decreased in size for the used Pt25 catalyst and is not seen in either of the Pt75 samples, which can be attributed to the Pt dispersion in the samples, whereby the bridged sites are barely detected in samples with poor dispersion [49]. This observation is in agreement with the TEM images shown in Figure 3, whereby Pt75 shows agglomeration of the particles. TEM carried out on both the Pt25 and Pt75 samples after reaction is shown in the SI (Figure S6). For both samples the images appear to show similar agglomeration and dispersion after the reaction. Size analysis carried out on the Pt25 images showed an average of 2.36nm, slightly larger than that of the fresh catalyst (2.14nm) however on further analysis (Figures S7 and S8), the size distribution of the Pt25 sample is wider than in the fresh catalyst, indicating that the Pt nanoparticles are modified during the reaction.

The peak at 2121 cm^{-1} appears only on the Pt25 catalyst before the reaction. Previous work suggests that this peak may be due to either oxidised species or CO adsorbed on platinum that is interacting with the Al_2O_3 support [48]. This analysis is backed up by EXAFS data performed on the fresh catalysts before reduction, whereby Pt25 showed a more pronounced feature corresponding to a Pt-O scattering interaction (Figure S9).

A fifth peak at 1972 cm^{-1} appears on the used catalyst samples. As this cannot be attributed to the interaction with Pt, it may be from a adsorbed product on the surface of the catalyst. We note that this peak is more prominent on the Pt25 sample, which may explain the deactivation seen in the Pt25 sample compared to the continuing activity of the Pt75.

Both used catalysts were also studied by EXAFS and compared to the results from the fresh catalysts, both in the synthesised (fresh) and reduced states. The used samples were pelletised after drying in air at 120°C and did not undergo any reduction treatments. From the results in Figure 11, the fresh Pt25 sample showed a peak at ~1.7 Å, assigned as the Pt-O scattering distance, demonstrating that the sample was partially oxidised. This peak decreased

in both the used and reduced samples, thereby indicating that the sample was reduced during the reaction. Not only was it reduced, but it did not reoxidise on exposure to air. This fact suggests that the sites on the Pt25 catalyst are blocked during reaction rather than restructuring of the surface. Further evidence for the Pt oxidation states of the Pt25 sample is seen in the height of the main edge feature in the XANES analysis (Figure 12). The fresh Pt25 sample shows the largest height, which can be attributed to the presence of oxidised Pt. The used sample is consistent with the sample analysed after reduction.

In comparing the fresh (reduced) and used samples, we can infer that in the Pt25 sample the Pt particles have increased in particle size, shown by an increase in the Pt-Pt scattering interaction at ~2.75 Å. Again, these results are in agreement with the IR studies, which showed fewer edge sites for the Pt25 catalyst after reaction. For the Pt75 catalyst, the results showed that the fresh sample was only slightly oxidised compared to the Pt25 catalyst and that there did not appear to be any particle size changes after reaction, confirming what is shown in the CO absorption analysis.

The characterisation of the used catalysts can be linked to the reusability testing of the Pt25 catalyst. As seen in Figure 9, the glycerol conversion shows an increase after the first reaction, this could be due to 2 factors; i) the catalyst is reduced *in situ* in the first cycle, causing an initial increase in activity before sites are then blocked or, ii) the Pt nanoparticles increase in size under the experimental conditions at 240°C. In Figure 4 we show that the glycerol conversion increased with increasing particle size up to around 3.5 nm, we can therefore conclude that there is a relation between the increase in activity with increasing particle size.

ATR-FTIR was used to characterize the Pt25 and Pt75 samples before and after the reforming reaction with glycerol. Figure 13 shows the resulting IR spectra. There are 3 bands marked with a * that appear in both samples after the reaction. These can be attributed to the boehmite form of alumina. The bands at 3323 cm^{-1} and 3085 cm^{-1} are assigned to AlOOH and the band at 1068 cm^{-1} to the AlOH bending vibration [50]. XRD analysis was also carried out on the Pt25 sample (Figure 14) where several new peaks have appeared in the used sample (marked *). The peaks at 2θ = 14.5°, 28.2°, 38.3°, 49.5°, 65.0° and 72.0° have been assigned to the boehmite form of alumina [46], therefore backing up the infrared data that the phase changes under APR conditions.

As the alumina phase changes to boehmite, this will result in a loss of surface area and accessible active sites, therefore will cause decrease of the catalytic activity, as shown in the reusability results. The ATR data shows that both the Pt25 and Pt75 samples change, therefore it is expected any contribution to the reaction pathway will be seen in both catalysts and comparisons can still be drawn. As there is a question over whether the formation of boehmite is delayed by the presence of metal particles [46], this is a topic that warrants further investigation to understand how the alumina phase change may affect the reaction profile of the APR of glycerol.

4. Conclusions

On systematically investigating the catalytic performance of supported Pt nanoparticles with a variation of Pt particle size in the aqueous reforming of glycerol, we found that an increase in particle size not only led to a higher conversion, but also selectively changed the reaction pathway to produce a different product distribution, showing a higher amount of liquid products such as 1,2-PDO. These results show that the conversion of glycerol on Pt catalysts with Pt particle size in the range 2 – 3.6 nm is structural sensitive, and a minor change of particle size significantly affects activity as well as yield to gas and liquid phase products.

Timed studies and further investigation into the complex network of reactions under APR conditions conformed schemes presented previously in the literature. Analysis of the catalysts after reaction allowed insight into the surface chemistry whereby links could be drawn between specific catalytic sites or conditions and differing reaction pathways described as:

a) Edge sites, such as Pt (100), prominent on small Pt particles – Responsible for the dehydrogenation of glycerol to glyceraldehyde in the reforming process, producing H_2 as the main product.
b) Facet sites (Pt (111)) prominent on large Pt particles – Responsible for the dehydration of glycerol to hydroxyacetone, leading to 1,2-Propanediol.
c) APR conditions in absence of ‘active’ catalyst – Responsible for reforming and hydrogenolysis of hydroxyacetone to form acetic acid and ethanol.

In summary, we have shown that careful consideration of the synthesis of Pt/Al_2O_3 catalysts can be used to fine tune the APR of glycerol to the desired products either for the formation of useful oxygenated liquid chemicals or gas phase products.

Although out with the scope of this study, in the near future we will focus on the development of Pt-based bimetallic catalysts, introducing transition metals such as Ni and Cu to act as promoters for the reaction.

Acknowledgements

UK Catalysis Hub is kindly thanked for resources and support provided via our membership of the UK Catalysis Hub Consortium and funded by EPSRC (grants EP/K014706/2, EP/K014668/1, EP/K014854/1, EP/K014714/1 and EP/M013219/1). This research has been performed with the use of facilities at the Research Complex at Harwell. The authors would like to thank Paul Collier at Johnson Matthey for his support and providing materials for the project. We would like to thank Gavin Stenning for help on the X-ray diffractometer in the Materials Characterisation Laboratory at the ISIS Neutron and Muon Source. Dr Emma Gibson and Ellie Dann are thanked for their help in the EXAFS and infrared measurements and data analysis. George Tierney is thanked for his help in preparing the TEM histograms.

References

[1] Y. Guo, M.U. Azmat, X. Liu, Y. Wang, G. Lu, Effect of support's basic properties on hydrogen production in aqueous-phase reforming of glycerol and correlation between WGS and APR, Appl. Energy. 92 (2012) 218–223.

[2] G. Wen, Y. Xu, H. Ma, Z. Xu, Z. Tian, Production of hydrogen by aqueous-phase reforming of glycerol, Int. J. Hydrogen Energy. 33 (2008) 6657–6666.

[3] P. Tuza, R.L. Manfro, N.F.P. Ribeiro, M.M.V.M. Souza, Production of renewable hydrogen by aqueous-phase reforming of glycerol over Ni-Cu catalysts derived from hydrotalcite precursors, Renew. Energy. 1 (2014) 413–426.

[4] R.R. Davda, J.W. Shabaker, G.W. Huber, R.D. Cortright, J.A. Dumesic, A review of catalytic issues and process conditions for renewable hydrogen and alkanes by aqueous-phase reforming of oxygenated hydrocarbons over supported metal catalysts, Appl. Catal. B Environ. 56 (2005) 171–186.

[5] A.O. Menezes, M.T. Rodrigues, A. Zimmaro, L.E.P. Borges, M.A. Fraga, Production of renewable hydrogen from aqueous-phase reforming of glycerol over Pt catalysts supported on different oxides, Renew. Energy. 36 (2011) 595–599.

[6] P.D. Vaidya, A.E. Rodrigues, Glycerol reforming for hydrogen production: A review,

Chem. Eng. Technol. 32 (2009) 1463–1469.

[7] S. Adhikari, S.D. Fernando, A. Haryanto, Hydrogen production from glycerol: An update, Energy Convers. Manag. 50 (2009) 2600–2604.

[8] R.D. Cortright, R.R. Davda, J.A. Dumesic, Hydrogen from catalytic reforming of biomass-derived hydrocarbons in liquid water, Nature. 418 (2002) 964–967.

[9] A. Wawrzetz, B. Peng, A. Hrabar, A. Jentys, A.A. Lemonidou, J.A. Lercher, Towards understanding the bifunctional hydrodeoxygenation and aqueous phase reforming of glycerol, J. Catal. 269 (2010) 411–420.

[10] P.D. Vaidya, J.A. Lopez-Sanchez, Review of Hydrogen Production by Catalytic Aqueous-Phase Reforming, ChemistrySelect. 2 (2017) 6563–6576.

[11] G.W. Huber, J.W. Shabaker, J.A. Dumesic, Raney Ni-Sn Catalyst for H2 Production from Biomass-Derived Hydrocarbons, Science (80-.). 300 (2003) 2075–2078.

[12] R.R. Davda, J.W. Shabaker, G.W. Huber, R.D. Cortright, J.A. Dumesic, Aqueous-phase reforming of ethylene glycol on silica-supported metal catalysts, Appl. Catal. B Environ. 43 (2003) 13–26.

[13] N.D. Subramanian, J. Callison, C.R.A. Catlow, P.P. Wells, N. Dimitratos, Optimised hydrogen production by aqueous phase reforming of glycerol on Pt/Al2O3, Int. J. Hydrogen Energy. 41 (2016) 18441–18450.

[14] G.W. Huber, J.A. Dumesic, An overview of aqueous-phase catalytic processes for production of hydrogen and alkanes in a biorefinery, Catal. Today. 111 (2006) 119–132.

[15] H. Bönnemann, G. Braun, W. Brijoux, R. Brinkmann, A.S. Tilling, K. Seevogel, K. Siepen, Nanoscale colloidal metals and alloys stabilized by solvents and surfactants Preparation and use as catalyst precursors, J. Organomet. Chem. 520 (1996) 143–162.

[16] F.L.S. Purgato, L.A. Montoro, J. Ribeiro, K.B. Kokoh, P. Olivi, The Effect of Heat Treatment on the Preparation of Pt-RuO2/C Electrocatalysts, Electrocatalysis. 1 (2010) 122–128.

[17] N. Dimitratos, J.A. Lopez-Sanchez, D. Morgan, A.F. Carley, R. Tiruvalam, C.J. Kiely, D. Bethell, G.J. Hutchings, Solvent-free oxidation of benzyl alcohol using Au-Pd

catalysts prepared by sol immobilisation, Phys. Chem. Chem. Phys. 11 (2009) 5142–53.

[18] L. Longenberger, G. Mills, Physical chemistry of ionic liquids, Phys. Chem. Chem. Phys. 12 (2010) 1648.

[19] S. Singh, J. Datta, Size control of Pt nanoparticles with stabilizing agent for better utilization of the catalyst in fuel cell reaction, J. Mater. Sci. 45 (2010) 3030–3040.

[20] S.M. Rogers, C.R.A. Catlow, C.E. Chan-Thaw, D. Gianolio, E.K. Gibson, A.L. Gould, N. Jian, A.J. Logsdail, R.E. Palmer, L. Prati, N. Dimitratos, A. Villa, P.P. Wells, Tailoring Gold Nanoparticle Characteristics and the Impact on Aqueous-Phase Oxidation of Glycerol, ACS Catal. 5 (2015) 4377–4384.

[21] C.-J. Jia, F. Schüth, Colloidal metal nanoparticles as a component of designed catalyst, Phys. Chem. Chem. Phys. 13 (2011) 2457–2487.

[22] T. Teranishi, M. Hosoe, T. Tanaka, M. Miyake, Size control of monodispersed Pt nanoparticles and their 2D organization by electrophoretic deposition, J. Phys. Chem. B. 103 (1999) 3818–3827.

[23] S.M. Rogers, C.R.A. Catlow, C.E. Chan-Thaw, A. Chutia, N. Jian, R.E. Palmer, M. Perdjon, A. Thetford, N. Dimitratos, A. Villa, P.P. Wells, Tandem Site- and Size-Controlled Pd Nanoparticles for the Directed Hydrogenation of Furfural, ACS Catal. 7 (2017) 2266–2274.

[24] F. Mauriello, A. Vinci, C. Espro, B. Gumina, M.G. Musolino, R. Pietropaolo, Hydrogenolysis vs. aqueous phase reforming (APR) of glycerol promoted by a heterogeneous Pd/Fe catalyst, Catal. Sci. Technol. 5 (2015) 4466–4473.

[25] D. Roy, B. Subramaniam, R. V. Chaudhari, Aqueous phase hydrogenolysis of glycerol to 1,2-propanediol without external hydrogen addition, Catal. Today. 156 (2010) 31–37.

[26] M.A. Dasari, P.P. Kiatsimkul, W.R. Sutterlin, G.J. Suppes, Low-pressure hydrogenolysis of glycerol to propylene glycol, Appl. Catal. A Gen. 281 (2005) 225–231.

[27] R.L. Maglinao, B.B. He, Verification of propylene glycol preparation from glycerol via the acetol pathway by in situ hydrogenolysis, Biofuels. 3 (2012) 675–682.

[28] N. Dimitratos, C. Messi, F. Porta, L. Prati, A. Villa, Investigation on the behaviour of Pt(0)/carbon and Pt(0),Au(0)/carbon catalysts employed in the oxidation of glycerol with molecular oxygen in water, J. Mol. Catal. A Chem. 256 (2006) 21–28.

[29] M. Comotti, W.C. Li, B. Spliethoff, F. Schüth, Support effect in high activity gold catalysts for CO oxidation, J. Am. Chem. Soc. 128 (2006) 917–924.

[30] A. Guinier, X-Ray Diffraction: In Crystals, Imperfect Crystals, and Amorphous Bodies, Dover Publications Inc., New York, 1994.

[31] B. Ravel, M. Newville, ATHENA, ARTEMIS, HEPHAESTUS: data analysis for X-ray absorption spectroscopy using IFEFFIT, J. Synchrotron Radiat. 12 (2005) 537–541.

[32] M. Newville, IFEFFIT : interactive XAFS analysis and FEFF fitting, J. Synchrotron Radiat. 8 (2001) 322–324.

[33] A.J. Bridgeman, Modeling the vibronic spectra of transition metal complexes: The ligand-field spectrum of [PtCl4]2-, Inorg. Chem. 47 (2008) 4817–4825.

[34] J.A. Creighton, D.G. Eadon, Ultraviolet–visible absorption spectra of the colloidal metallic elements, J. Chem. Soc. Faraday Trans. 87 (1991) 3881–3891.

[35] A. Miyazaki, I. Balint, Y. Nakano, Morphology Control of Platinum Nanoparticles and their Catalytic Properties, J. Nanoparticle Res. 5 (2003) 69–80.

[36] C. Bock, C. Paquet, M. Couillard, G.A. Botton, B.R. MacDougall, Size-selected synthesis of PtRu nano-catalysts: Reaction and size control mechanism, J. Am. Chem. Soc. 126 (2004) 8028–8037.

[37] P. Scherrer, Bestimmung der Größe und der inneren Struktur von Kolloidteilchen mittels Röntgenstrahlen, Nachr. Ges. Wiss. Göttingen. 26 (1918) 98–100.

[38] A.M. Beale, B.M. Weckhuysen, EXAFS as a tool to interrogate the size and shape of mono and bimetallic catalyst nanoparticles, Phys. Chem. Chem. Phys. 12 (2010) 5562–5574.

[39] N. Luo, X. Fu, F. Cao, T. Xiao, P.P. Edwards, Glycerol aqueous phase reforming for hydrogen generation over Pt catalyst - Effect of catalyst composition and reaction conditions, Fuel. 87 (2008) 3483–3489.

[40] Z. Wei, A. Karim, Y. Li, Y. Wang, Elucidation of the Roles of Re in Aqueous-Phase Reforming of Glycerol over Pt-Re/C Catalysts, ACS Catal. 5 (2015) 7312–7320.

[41] N. Luo, X. Zhao, F. Cao, T. Xiao, D. Fang, Thermodynamic study on hydrogen generation from different glycerol reforming processes, Energy and Fuels. 21 (2007) 3505–3512.

[42] R. Sundari, P.D. Vaidya, Reaction Kinetics of Glycerol Steam Reforming Using a Ru/Al2O3 Catalyst, Energy & Fuels. 26 (2012) 4195–4204.

[43] C.H. Zhou, H. Zhao, D.S. Tong, L.M. Wu, W.H. Yu, Recent Advances in Catalytic Conversion of Glycerol, Catal. Rev. 55 (2013) 369–453.

[44] M. El Doukkali, A. Iriondo, J.F. Cambra, I. Gandarias, L. Jalowiecki-Duhamel, F. Dumeignil, P.L. Arias, Deactivation study of the Pt and/or Ni-based gamma-Al 2 O 3 catalysts used in the aqueous phase reforming of glycerol for H 2 production, Appl. Catal. A Gen. 472 (2014) 80–91.

[45] G.F. Wei, Z.P. Liu, Restructuring and Hydrogen Evolution on Pt Nanoparticle, Chem. Sci. 6 (2015) 1485–1490.

[46] R.M. Ravenelle, J.R. Copeland, A.H. Van Pelt, J.C. Crittenden, C. Sievers, Stability of Pt/γ-Al2O3catalysts in model biomass solutions, Top. Catal. 55 (2012) 162–174.

[47] N. Sheppard, T.T. Nguyen, Advances in Infrared and Raman Spectroscopy, in: R. J. H. Clark, R. E. Hester (Eds.), Adv. Infrared Raman Spectrosc., Heyden, London, 1978: p. 67.

[48] R. Barth, R. Pitchai, R.L. Anderson, X.E. Verykios, Thermal desorption-infrared study of carbon monoxide adsorption by alumina-supported platinum, J. Catal. 116 (1989) 61–70.

[49] J.M.C. Bueno, B.A. Riguetto, S. Damyanova, G. Gouliev, C.M.P. Marques, L. Petrov, Surface Behavior of Alumina-Supported Pt Catalysts Modified with Cerium as Revealed by X-ray Diffraction , X-ray Photoelectron Spectroscopy , and Fourier Transform Infrared Spectroscopy of CO Adsorption, J. Phys. Chem. B. 108 (2004) 5349–5358.

[50] D.A. Boga, F. Liu, P.C.A. Bruijnincx, B.M. Weckhuysen, Aqueous-phase reforming of crude glycerol: effect of impurities on hydrogen production, Catal. Sci. Technol. 6

(2016) 134–143.

Tables, Figures and Schemes

Table 1. Characterisation of Pt/Al_2O_3 catalysts produced using the colloidal method at various temperatures.

Pt/Al_2O_3 Sample	Pt-Pt Coordination Number	Particle Size, nm		
		EXAFS	TEM	XRD
Pt 25	8.7 (5)	1.54	2.14	2.25
Pt 50	9.5 (4)	1.97	[b]	2.88
Pt 75	10.6 (3)	[a]	[b]	3.48
Pt 90	11.1 (4)	[a]	[b]	3.61

[a]Size calculation limited to coordination number <10
[b]\Data could not be calculated due to agglomeration in samples

Table 2. Conversion of several reactants over 2% Pt/Al_2O_3 (Pt25) catalyst. Reaction conditions: 240°C, PAr = 42 bar, 1000 rpm, 60 mg catalyst, 1 h reaction time.

Reactant	Reactant concentration, wt%	Reactant conversion, %
Glycerol (GL)	10	8.8
Hydroxyacetone (HA)	10	52.9
1,2-Propanediol (1,2-PDO)	10	22.0
Lactic Acid (LA)	10	2.7
Glyceraldehyde (GA)	1	100.0

Table 3. Infrared assignments for Pt25 and Pt75 fresh and used catalysts after CO adsorption.

		Wavenumber, cm^{-1}			
Peak	Assignment	Pt25 Fresh	Pt25 Used	Pt75 Fresh	Pt75 Used
I	Oxidised species	2121	-	-	-
II	Linear CO on Pt (111)	2084	2081	2089	2092
III	Linear CO on edge sites	2062	-	-	-
IV	Product interaction	-	1972	-	1975
V	Twofold bridge sites	1838	-	-	-

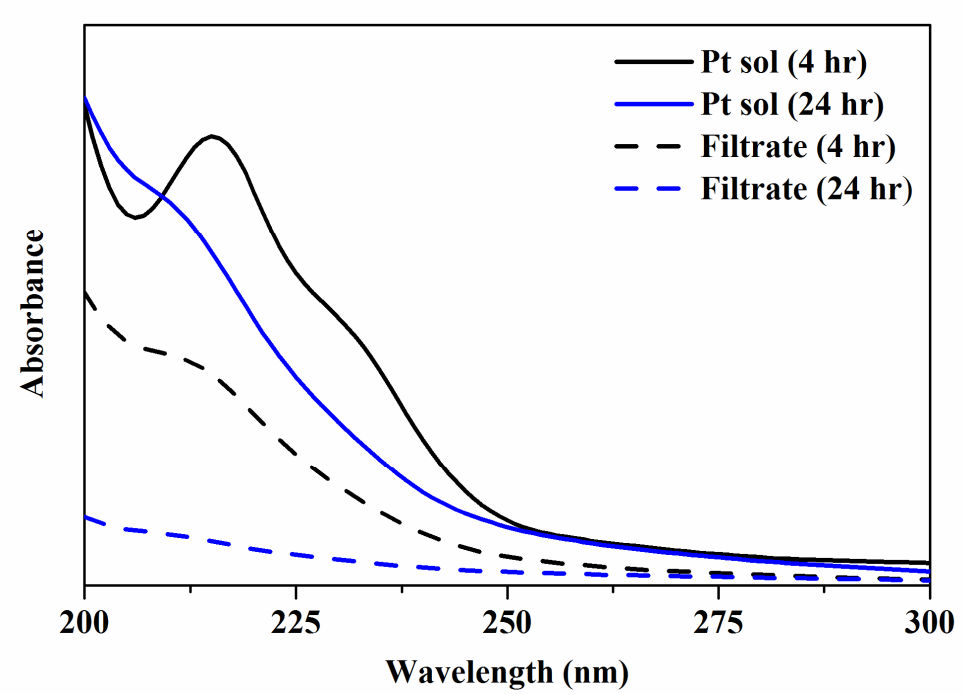

Figure 1. UV-Vis spectra of Pt sols after reduction with $NaBH_4$ for 4 hours and 24 hours, plus the respective filtrated solutions after immobilisation on Al_2O_3.

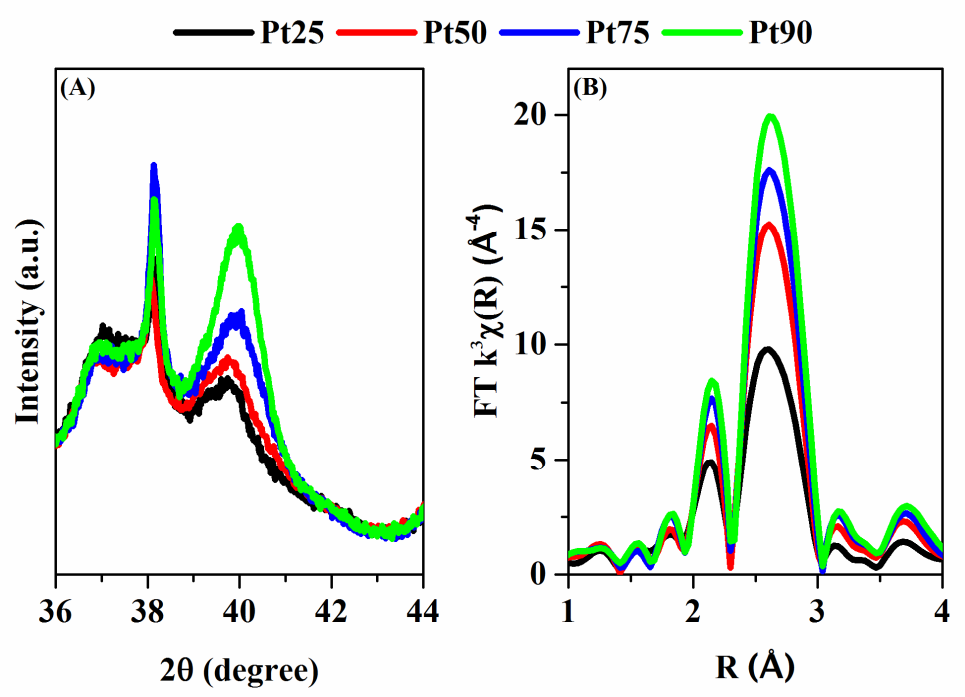

Figure 2. XRD (A) and EXAFS (B) analysis of 2% Pt/Al_2O_3 catalysts produced at different colloidal reduction temperatures, black – Pt25, red – Pt50, blue – Pt75, green – Pt90.

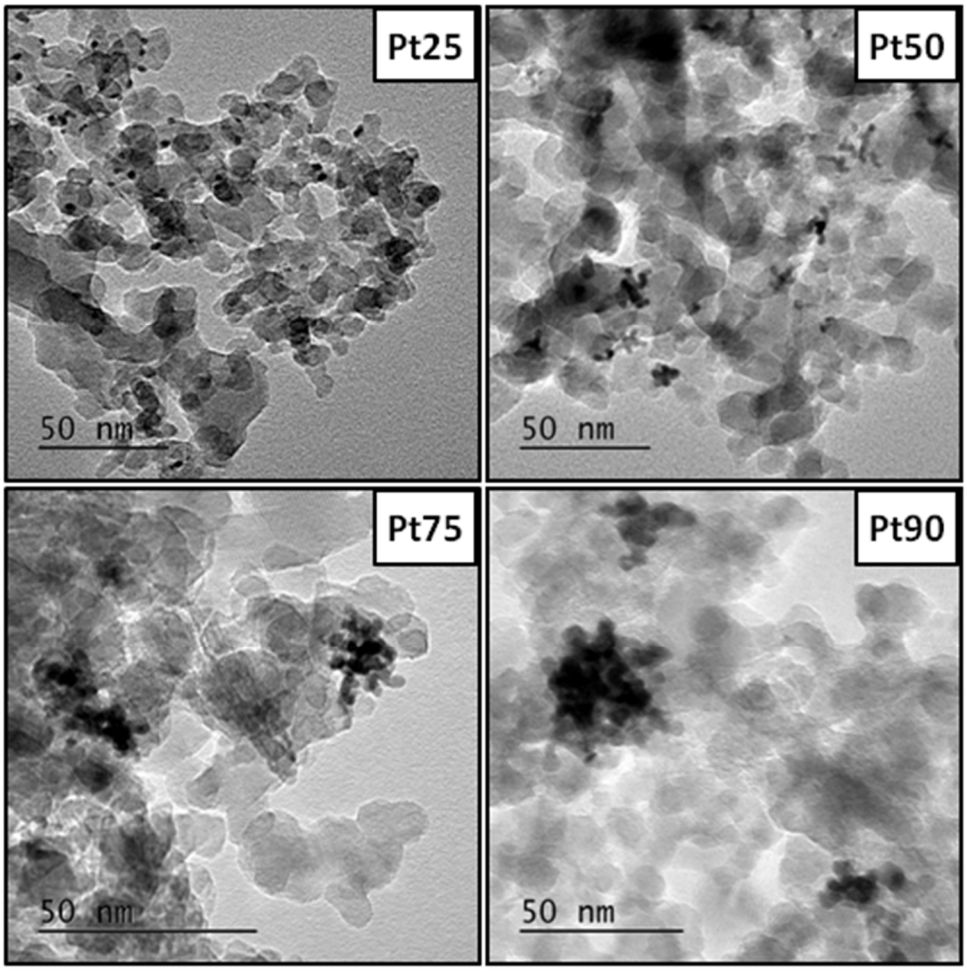

Figure 3. TEM images of catalyst samples Pt25 (top left), Pt50 (top right), Pt75 (bottom left) and Pt90 (bottom right) at 50nm scale.

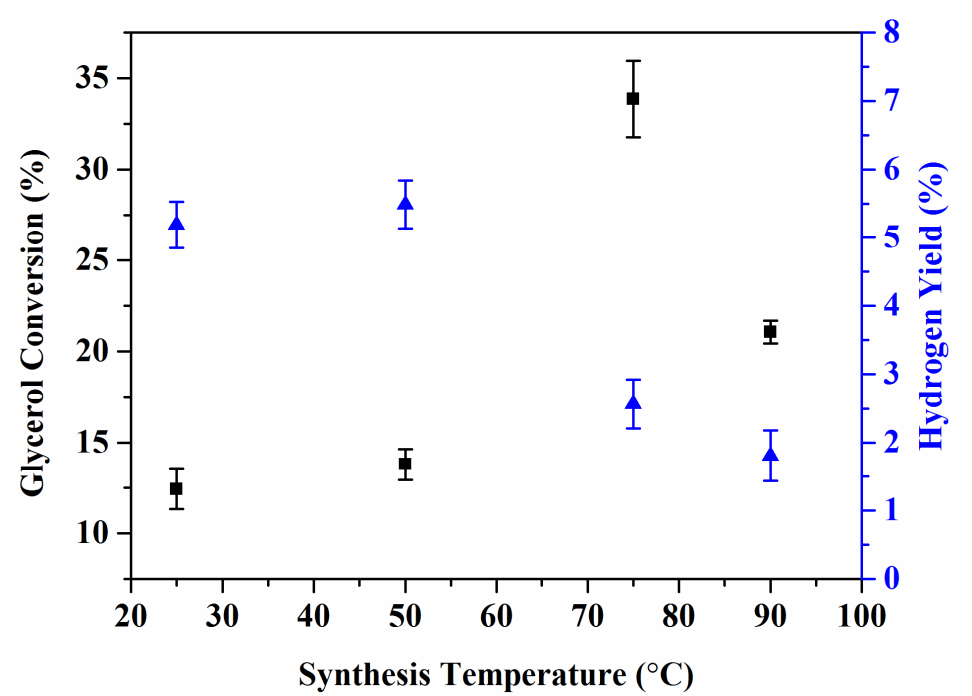

Figure 4. Glycerol conversion (■) and H_2 yield (▲) for 2% Pt/Al_2O_3 catalysts produced at different colloidal reduction temperatures. Reaction conditions: 240°C, P_{Ar} = 42 bar, 1000 rpm, 10 wt% glycerol, 60 mg catalyst, 2 h reaction time.

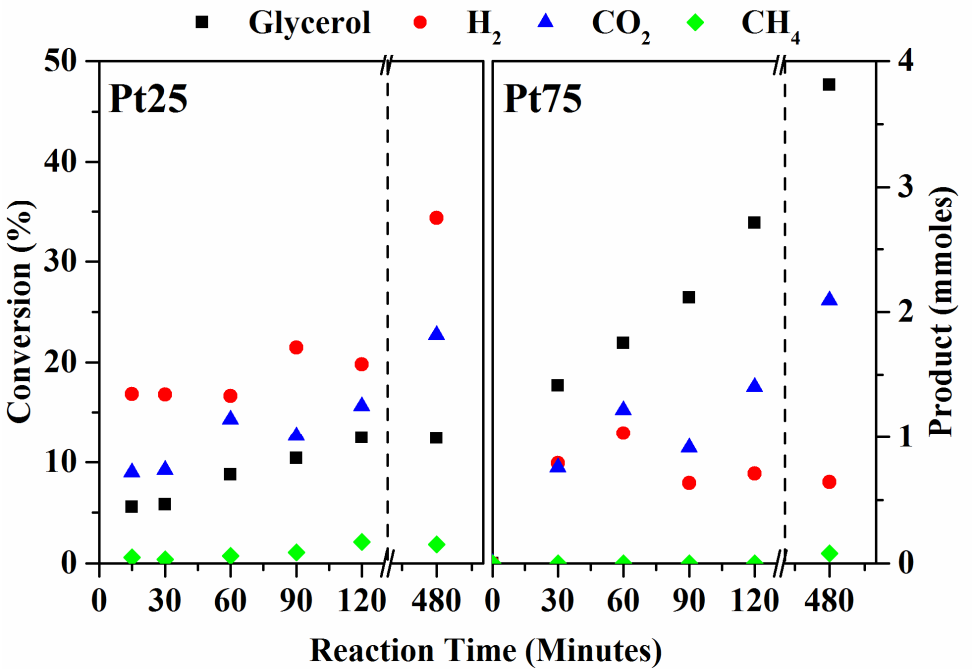

Figure 5. Glycerol conversion and gas products from APR of glycerol using Pt25 and Pt75 catalysts over various reaction times. Reaction conditions: 240°C, P_{Ar} = 42 bar, 1000 rpm, 10 wt% glycerol, 60 mg catalyst.

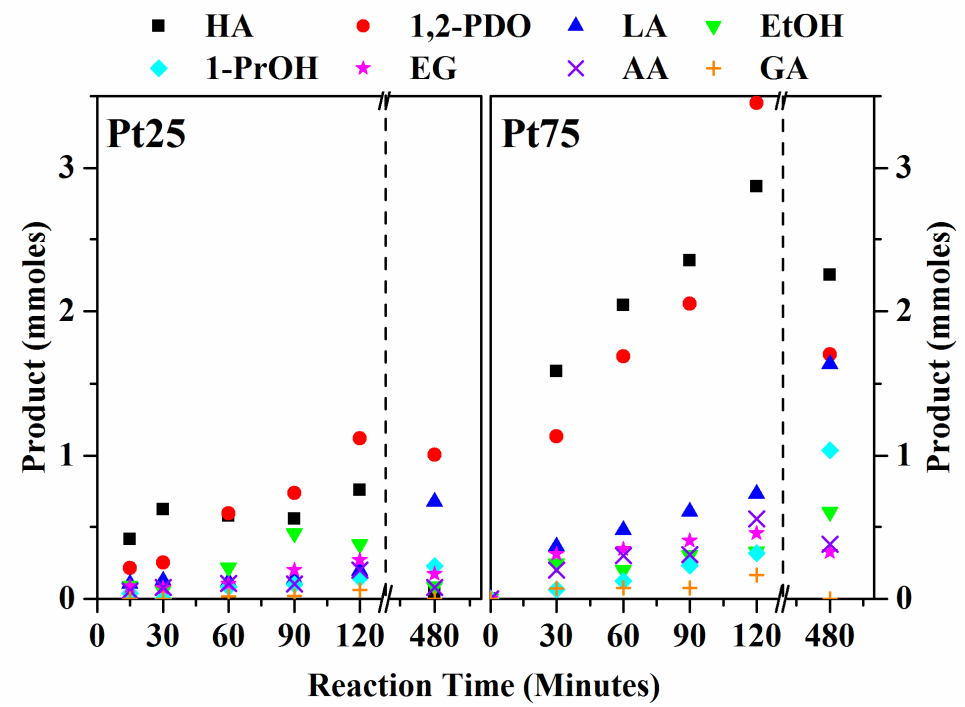

Figure 6. Major liquid products formed from APR of glycerol using Pt25 and Pt75 catalysts over various reaction times. Reaction conditions: 240°C, P_{Ar} = 42 bar, 1000 rpm, 10 wt% glycerol, 60 mg catalyst.

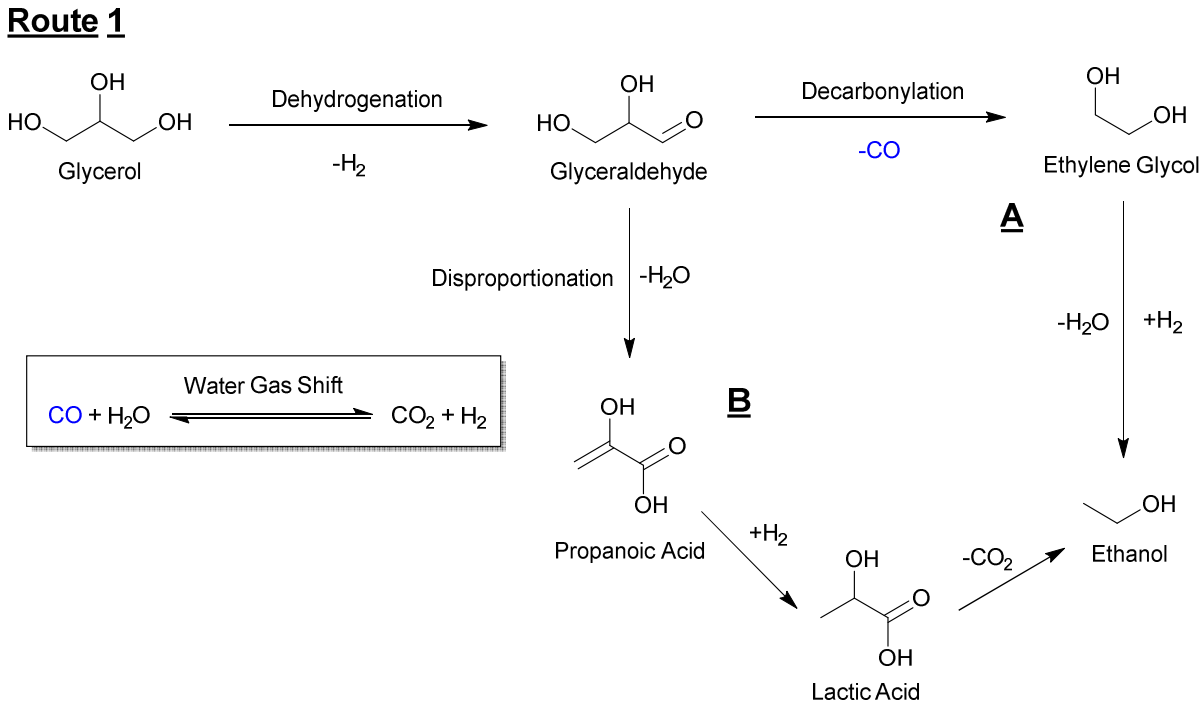

Scheme 1. Proposed reaction pathway for APR of glycerol – Route 1

Route 2

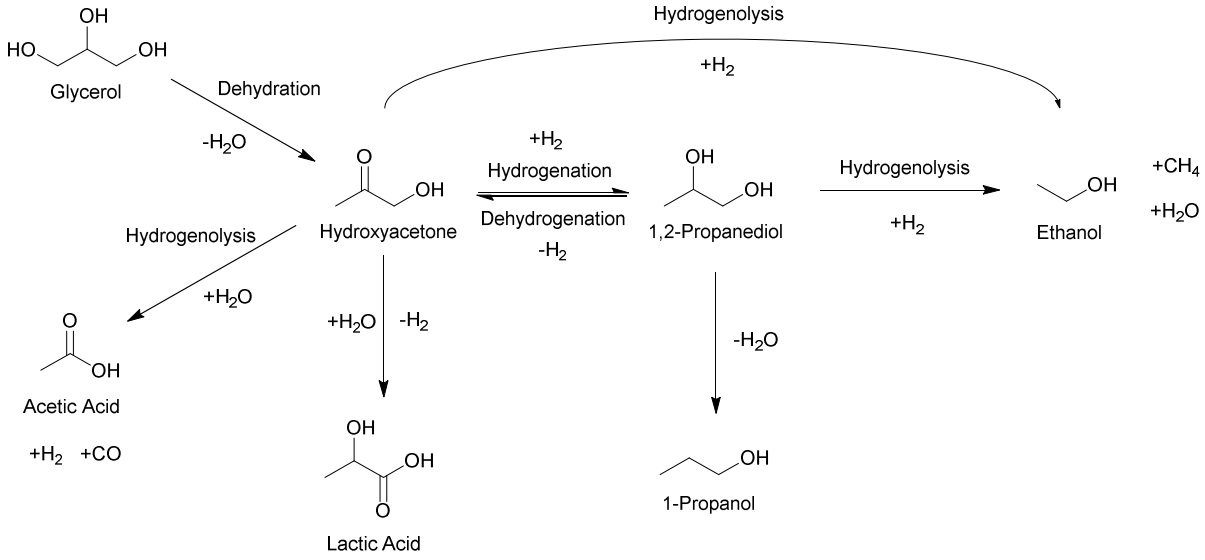

Scheme 2. Proposed reaction pathway for APR of glycerol – Route 2

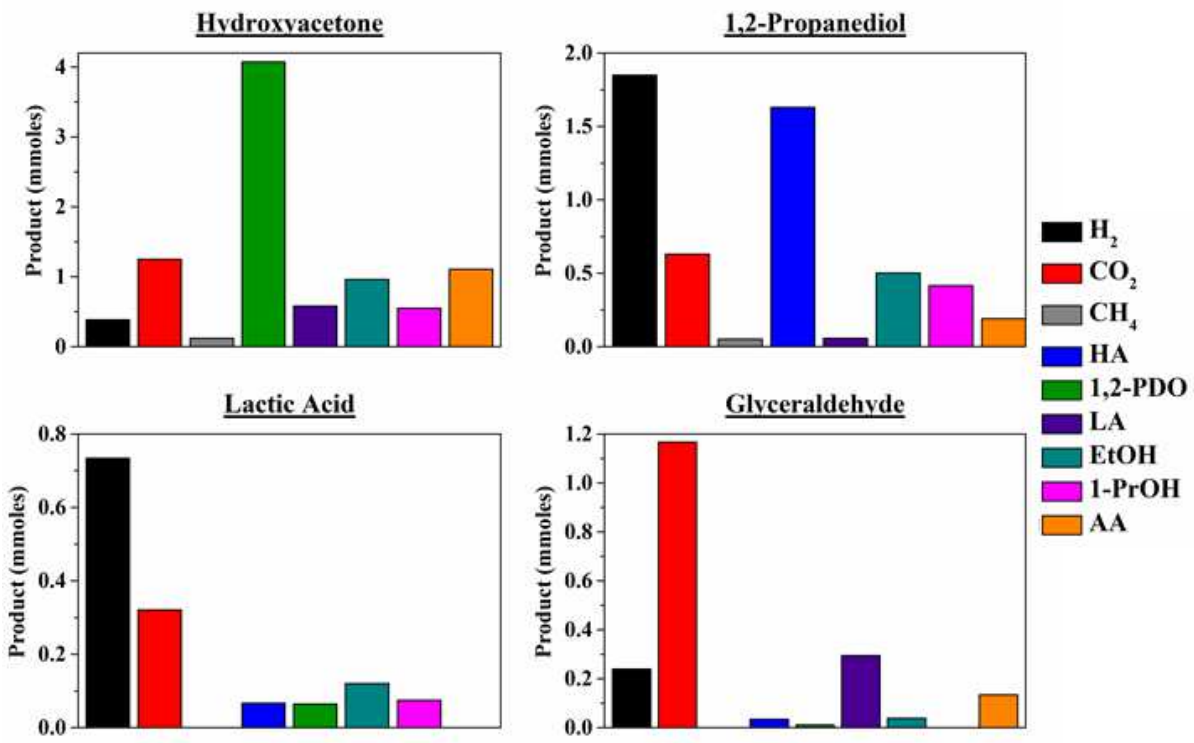

Figure 7. Product formation from intermediates over 2% Pt/Al_2O_3 (Pt25) catalyst. Reaction conditions: 240°C, PAr = 42 bar, 1000 rpm, 10 wt% reactant for HA, 1,2-PDO and LA, 1 wt% for Glyceraldehyde, 60 mg catalyst, 1 h reaction time.

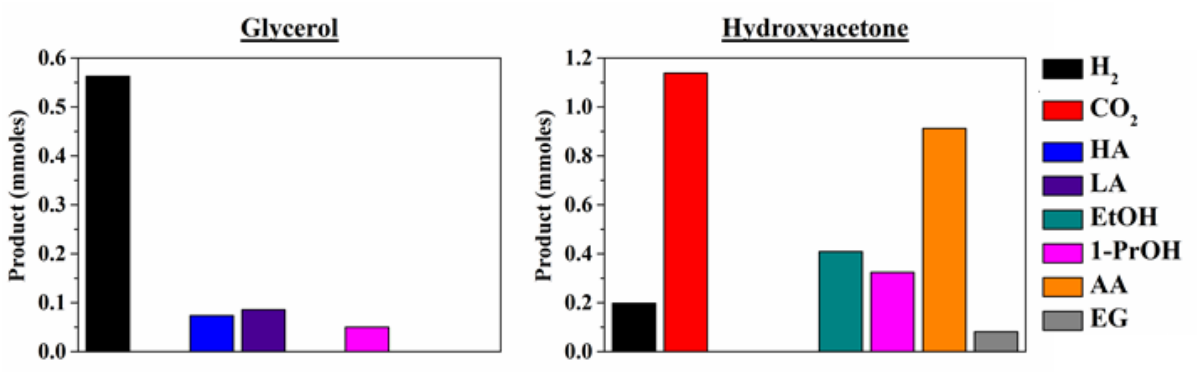

Figure 8. Product formation from glycerol and hydroxyacetone over Al_2O_3. Reaction conditions: 240°C, PAr = 42 bar, 1000 rpm, 10 wt% reactant, 60 mg catalyst, reaction time = 2hr for glycerol, 1h for hydroxyacetone.

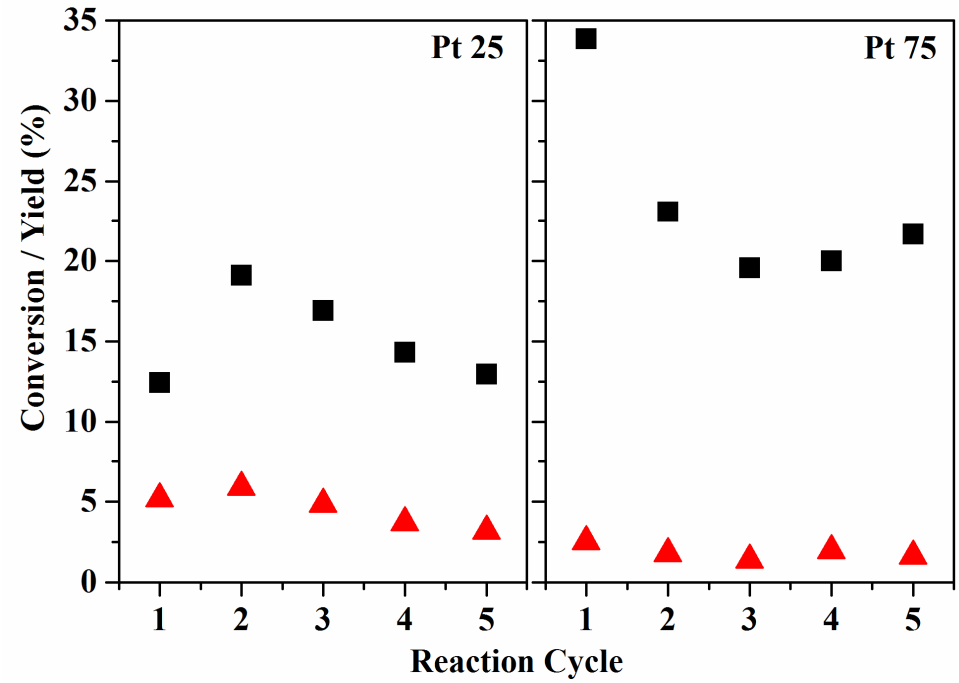

Figure 9. Glycerol conversion (■) and H_2 yield (▲) for 2% Pt/Al_2O_3 catalysts produced at 25°C and 75°C. Reaction conditions: 240°C, PAr = 42 bar, 1000 rpm, 10 wt% glycerol, 60 mg catalyst, 2 h reaction time.

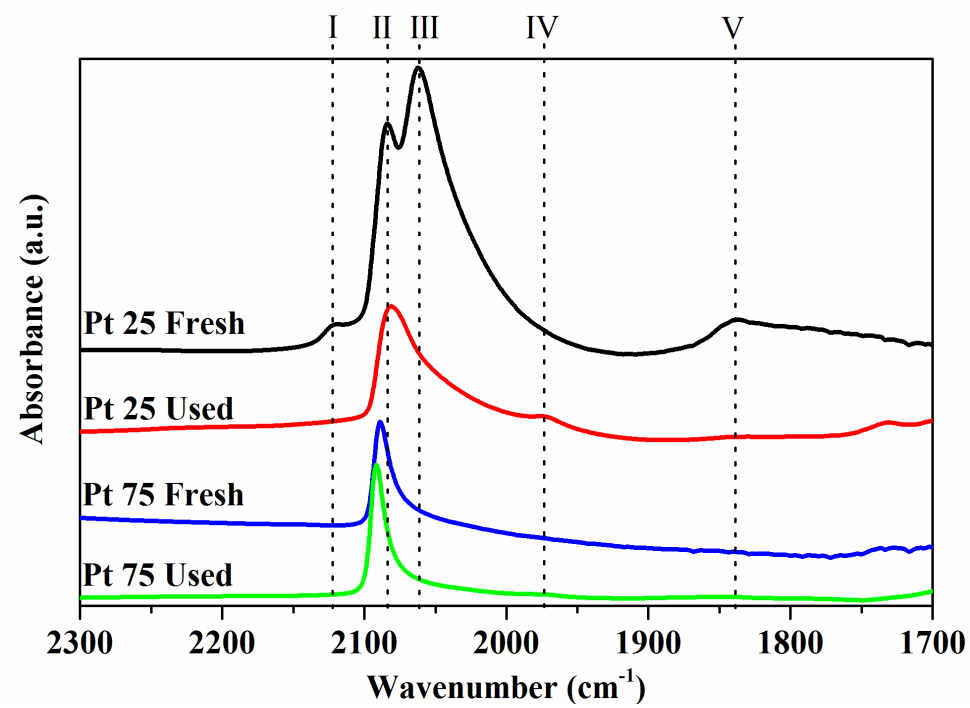

Figure 10. CO adsorption coverage of Pt25 and Pt75 catalysts before and after one reaction cycle of 2 hours.

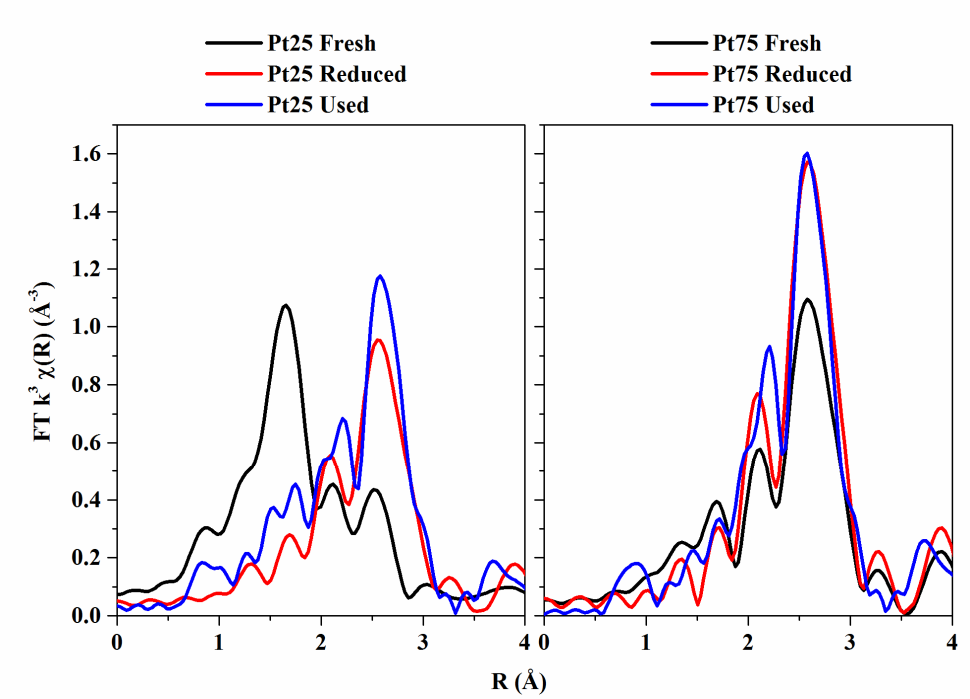

Figure 11. EXAFS analysis of Pt25 and Pt75 catalysts in the fresh, reduced and used states.

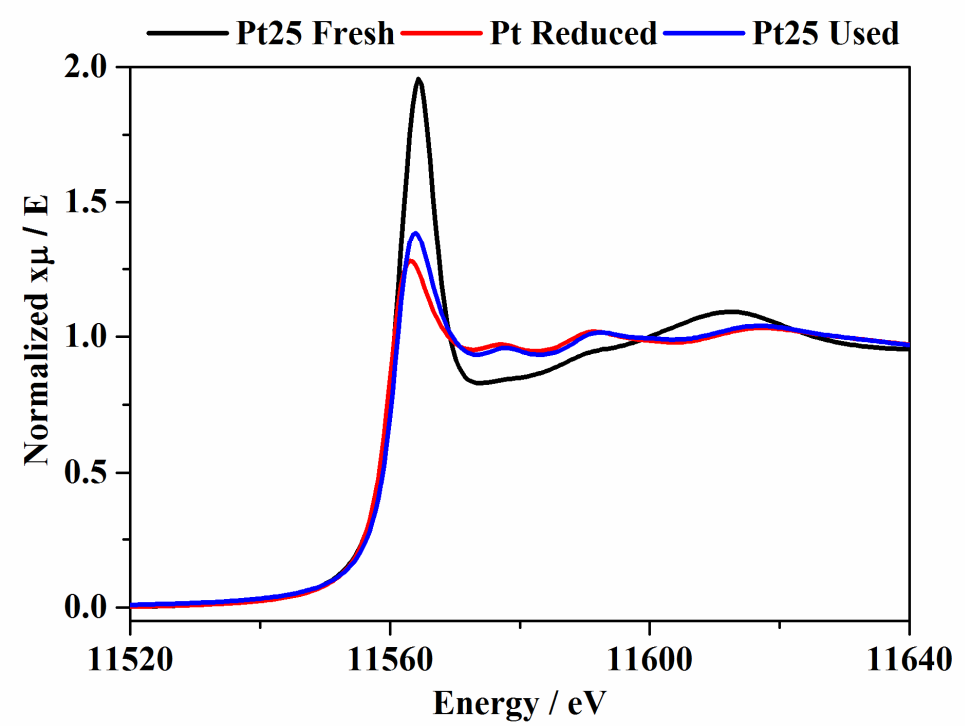

Figure 12. Normalised XANES spectra of Pt25 in the fresh, reduced and used states.

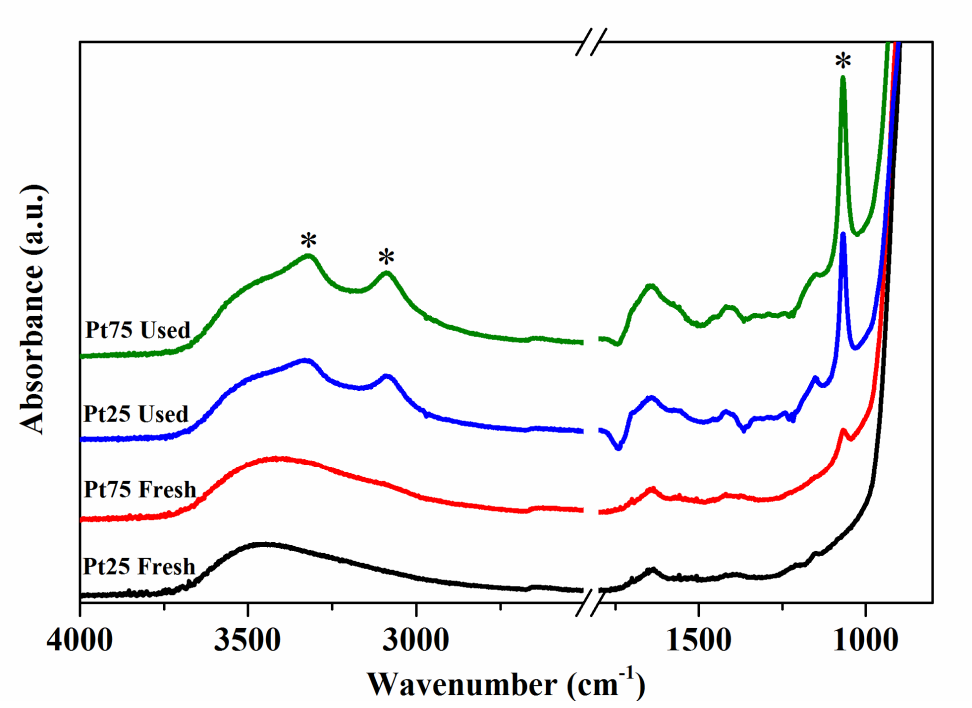

Figure 13. ATR-FTIR Spectra of Pt25 and Pt75 samples before and after aqueous-phase glycerol reforming reaction.

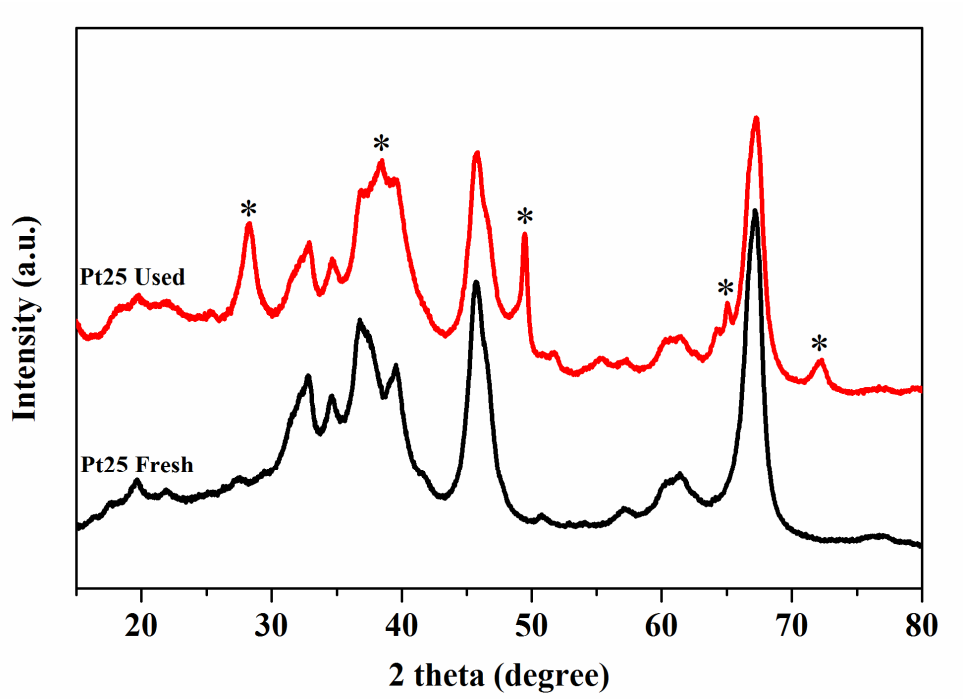

Figure 14. XRD patterns of Pt25 before (fresh) and after (used) aqueous-phase glycerol reforming reaction.